Band renormalization and Fermi surface reconstruction in iron-based superconductors

Shun-Li Yu, Jing Kang, and Jian-Xin Li
Department of Physics and National Laboratory of Solid State Microstructures, Nanjing University, Nanjing 210093, China
(Received 2 November 2008; revised manuscript received 6 January 2009; published 17 February 2009)

Using the fluctuation exchange approximation and a three-orbital model, we study the band renormalization, the Fermi surface reconstruction, and the superconducting pairing symmetry in iron-based superconductors. We find that the interorbital spin fluctuations lead to the strong anisotropic band renormalization and the renormalization is orbital dependent. As a result, the topology of Fermi surface displays distinct variation with doping from the electron type to the hole type, which is consistent with the recent experiments. This shows that the Coulomb interactions will have a strong effect on the band renormalization and the topology of the electron Fermi pocket. In addition, the pairing state mediated by the interorbital spin fluctuation is of an extended *s*-wave symmetry.

DOI: 10.1103/PhysRevB.79.064517 PACS number(s): 74.70.−b, 74.25.Jb, 71.18.+y, 74.20.Mn

I. INTRODUCTION

Recently, the discovery of superconductivity in the iron-based compounds has generated enormous interest because these materials are the noncopper superconductors with high superconducting (SC) critical temperature. These compounds share the same FeAs (or FeP) layers that are believed to be responsible for the superconductivity. Two classes of such compounds have been extensively investigated. (1) The LaOFeAs classes (denoted as FeAs-1111), space group P_4/mmm, with $T_c \approx 26$ K through electron doping with replacing O^{2-} by F^- (Ref. 1) and T_c can be up to about 41–56 K by replacing lanthanum by other rare-earth ions.[2–4] (2) The $BaFe_2As_2$ classes (denoted as FeAs-122), space group I_4/mmm, with $T_c \approx 38$ K through hole doping with substituting Ba^{2+} for K^+.[5] All parent compounds show a spin-density-wave (SDW) abnormality below a temperature ~150 K (Refs. 6–9) and the superconductivity is associated with the suppression of the SDW. Most experiment measurements have shown that these superconductors open a full gap around both the hole and electron Fermi pockets[10–15] though the NMR[16,17] and transport[18,19] experiments suggest the presence of gap nodes. At the same time, although the angle-resolved photoemission spectroscopy (ARPES) measurements of the band structure and Fermi surface (FS) in the undoped and electron-doped samples[20–22] are qualitatively in agreement with the finding of the first-principle band calculation,[23,24] a strong anisotropic band renormalization is found. On the other hand, the ARPES data for the hole-doped FeAs-122 reveal the electron FS around (π,π) consisting of disconnecting patches,[15,25] which exhibits a significant difference from the result obtained in the band-structure calculation. Therefore, the understanding of the role played by the electron correlation and the origin of the different electron FS topology between the hole-doped and electron-doped system is of importance.

As the band-structure calculations have shown, the FS and band structures of these compounds are qualitatively similar[23,24,26] and the Fe 3*d* orbitals represent the main contribution to the density of states, together with a contribution from As *p* orbitals, within several eV of the Fermi level. In the FeAs layers, the Fe atoms form a square lattice and an Fe atom is coordinated by four As atoms in a tetrahedron. Due to the direct Fe-Fe bonds and the hybridization with the As 4*p* orbitals, the Fe 3*d* orbitals form a complex band structure. However, the main contribution to the bands near the Fermi level comes from the d_{xz}, d_{yz}, and the d_{xy} orbitals (the direct Fe-Fe bonds along the *x* and *y* axes) of the Fe atoms.[26–28] In this paper, we employ a three-orbital (the d_{xz}, d_{yz}, and d_{xy} orbitals) model[29] to investigate the band renormalization, FS reconstruction, and superconducting gap symmetry in the iron-based compounds with the fluctuation exchange (FLEX) approximation. We find that a strong anisotropic band renormalization is resulted from the Coulomb interaction with the strongest effect occurring around the $\tilde{X}=(0,\pi)$ point, which is defined in the unfolded Brillouin zone (BZ), and this renormalization increases rapidly with the increase in the Hund's coupling J when $J>0.18U$ (U is the intraorbital Coulomb interaction). Due to the band renormalization, the Fermi level for the undoped case is slightly below the flatband centered around the $\tilde{X}$ point which is the bottom of the band along the $\tilde{\Gamma}=(0,0)$ to $\tilde{X}$ direction. As a result, for the hole-doped case, the Fermi level will situate below the flatband along the $\tilde{\Gamma}$ to $\tilde{X}$ direction though it still crosses the renormalized band along the $\tilde{X}$ to $\tilde{M}=(\pi,\pi)$ direction. In this case, the FS around $\tilde{X}$ consists of disconnecting patches. However, in the electron-doped case, the Fermi level is lifted to be above the flatband and the circularlike FS is formed. This result provides a possible explanation for the different FS topology observed in the electron-doped and hole-doped materials. We also carry out the same calculation based on the two-orbital model;[30] no similar FS reconstruction has been found. This difference is ascribed to be due to the orbital-dependent renormalization. On the other hand, the most favored pairing state mediated by the interorbital spin fluctuations is found to be the extended *s* wave with a sign change between the electron and hole Fermi pockets, which is consistent with the result obtained in the two-orbital model.[31–35] This indicates that the two models share the similar physics as far as the pairing symmetry is concerned but exhibits difference in the band renormalization.

The paper is organized as follows. In Sec. II, we present the three-orbital model and discuss the FLEX method. In

Sec. III, the numerical results for the band renormalization is presented and discussed. We also give a brief discussion on the pairing symmetry in this section. In Sec. IV, we give a summary of the results.

II. MODEL AND FLEX METHOD

The model Hamiltonian consists of two parts,

$$H = H_0 + H_{\text{int}}, \tag{1}$$

where the bare Hamiltonian H_0 is given by the three-orbital model as introduced in Ref. 29. In the unfolded (extended) BZ for the reduced unit cell (only one Fe atom in the unit cell as in Ref. 27), it can be written as $H_0=\Sigma_k \Psi_k^\dagger M_k \Psi_k$ with

$$M_k = \begin{pmatrix} \varepsilon_{xz}(k+Q) & \varepsilon_{xz,yz}(k+Q) & \varepsilon_{xz,xy}(k) \\ \varepsilon_{xz,yz}(k+Q) & \varepsilon_{yz}(k+Q) & \varepsilon_{yz,xy}(k) \\ \varepsilon^*_{xz,xy}(k) & \varepsilon^*_{yz,xy}(k) & \varepsilon_{xy}(k) \end{pmatrix}, \tag{2}$$

and $\Psi_k=(c^{xz}_{k+Q}, c^{yz}_{k+Q}, c^{xy}_k)^T$. Here the diagonal elements of M_k denote the dispersion of Fe $3d$ orbitals d_{xz}, d_{yz}, and d_{xy}, while the others denote the hybridization among them. Keeping up to the next-nearest-neighbor hopping terms, we have $\varepsilon_{xz}(k) = -\Sigma_k[2t_1 \cos k_x + 2t_2 \cos k_y + 4t_3 \cos k_x \cos k_y]$, $\varepsilon_{yz}(k) = -\Sigma_k[2t_1 \cos k_y + 2t_2 \cos k_x + 4t_3 \cos k_x \cos k_y]$, $\varepsilon_{xy}(k) = -\Sigma_k[2t_4(\cos k_x + \cos k_y) + 4t_5 \cos k_x \cos k_y]$, $\varepsilon_{xz,yz}(k) = \varepsilon_{yz,xz}(k) = -\Sigma_k 4t_6 \sin k_x \sin k_y$, $\varepsilon_{xz,xy}(k) = \varepsilon^*_{xy,xz}(k) = -\Sigma_k 2it_7 \sin k_x$,[29] and $\varepsilon_{yz,xy}(k) = \varepsilon^*_{xy,yz}(k) = -\Sigma_k 2it_7 \sin k_y$,[29] In order to reproduce the FS and band-structure feature, we set the parameters as $t_1=-1.0$ (≈ 0.4 eV), $t_2=0.7$, $t_3=-0.8$, $t_4=-0.3$, $t_5=0.2$, $t_6=0.6$, and $t_7=-0.35$. As the three orbitals belong to the t_{2g} manifold, we set the same on-site energy to the three orbitals. In Fig. 1, we show the band structure and FS with $\mu=1.15$ (electron density per site $n=4.0$) corresponding to the parent compound. We find that this three-orbital model can basically reproduce the main features of the FS and band structure obtained in the local-density approximation (LDA) calculation.[23,24]

The interaction between electrons is included in H_{int} as follows:

$$\begin{aligned} H_{\text{int}} = & \frac{1}{2}U \sum_{i,l,\sigma\neq\sigma'} c^\dagger_{il\sigma} c^\dagger_{il\sigma'} c_{il\sigma'} c_{il\sigma} \\ & + \frac{1}{2}U' \sum_{i,l\neq l',\sigma,\sigma'} c^\dagger_{il\sigma} c^\dagger_{il'\sigma'} c_{il'\sigma'} c_{il\sigma} \\ & + \frac{1}{2}J \sum_{i,l\neq l',\sigma,\sigma'} c^\dagger_{il\sigma} c^\dagger_{il'\sigma'} c_{il\sigma'} c_{il'\sigma} \\ & + \frac{1}{2}J' \sum_{i,l\neq l',\ \sigma\neq\sigma'} c^\dagger_{il\sigma} c^\dagger_{il\sigma'} c_{il'\sigma'} c_{il'\sigma}, \end{aligned} \tag{3}$$

where $U(U')$ is the intraorbital (interorbital) Coulomb interaction, J is the Hund's coupling, and J' is the interorbital pair hopping.

We carry out the investigation using the FLEX approximation,[36] in which the Green's function and spin/charge fluctuations are determined self-consistently. For the three-orbital model, the Green's function $\hat{G}$ and the self-energy $\hat{\Sigma}$ are expressed in a 3×3-matrix form, while the susceptibility $\hat{\chi}^0$ and the effective interaction $\hat{V}$ have a 9×9-matrix form. The Green's function satisfies the Dyson equation $\hat{G}(k)^{-1}=\hat{G}^0(k)^{-1}-\hat{\Sigma}(k)$, where the self-energy is given by $\Sigma_{mn}(k)=\frac{T}{N}\Sigma_q\Sigma_{\mu\nu}V_{n\mu,m\nu}(q)G_{\mu\nu}(k-q)$ and the bare Green's function reads as $\hat{G}^0(k)=(i\omega_n-\hat{M}_k+\mu)^{-1}$. The fluctuation exchange interaction is given by

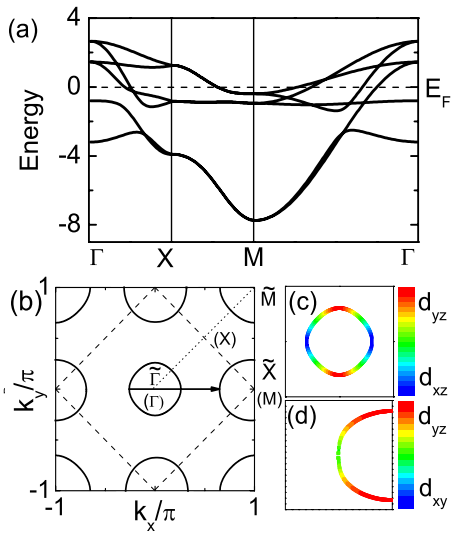

FIG. 1. (Color online) Band structure and FS of the three-orbital model. (a) The band structure in the folded BZ with $t_1=-1.0$, $t_2=0.7$, $t_3=-0.8$, $t_4=-0.3$, $t_5=0.2$, $t_6=0.6$, $t_7=0.35$, and $\mu=1.15$. (b) The FS in the unfolded BZ. The dashed lines denote the boundary of the folded BZ. The line with an arrow denotes the nesting vector between the hole and electron Fermi pockets. Panels (c) and (d) replot the hole and the electron Fermi pockets shown in (b), respectively, with the different colors representing the weight of the different orbitals.

$$\begin{aligned} V_{\mu m,n\nu}(q) = \frac{1}{2}\Big[& 3\hat{U}^s\hat{\chi}^s(q)\hat{U}^s + \hat{U}^c\hat{\chi}^c(q)\hat{U}^c - \frac{1}{2}(\hat{U}^s+\hat{U}^c)\hat{\chi}^0(q) \\ & \times(\hat{U}^s+\hat{U}^c) + 3\hat{U}^s - \hat{U}^c \Big]_{\mu m,n\nu}, \end{aligned} \tag{4}$$

with spin susceptibility $\hat{\chi}^s(q)=[\hat{I}-\hat{\chi}^0(q)\hat{U}^s]^{-1}\hat{\chi}^0(q)$ and charge susceptibility $\hat{\chi}^c(q)=[\hat{I}+\hat{\chi}^0(q)\hat{U}^c]^{-1}\hat{\chi}^0(q)$. The irreducible susceptibility is given by $\chi^0_{\mu m,n\nu}(q)=-\frac{T}{N}\Sigma_k G_{n\mu}(k+q)G_{m\nu}(k)$. In the above, T is temperature, $k\equiv(\mathbf{k},i\omega_n)$ with $\omega_n=\pi T(2n+1)$, and $\hat{I}$ is the identity matrix. The interaction matrix for the spin (charge) fluctuation $\hat{U}^s$ ($\hat{U}^c$) is given by: for $i=j=k=l$, $U^s_{ij,kl}=U$ ($U^c_{ij,kl}=U$); for $i=j\neq k=l$, $U^s_{ij,kl}=J$ ($U^c_{ij,kl}=2U'-J$); for $i=k$, $j=l$ and $i\neq j$, $U^s_{ij,kl}=U'$ ($U^c_{ij,kl}=-U'+2J$); for $i=l$, $j=k$ and $i\neq j$, $U^s_{ij,kl}=J$ ($U^c_{ij,kl}=J$); for other cases, $U^s_{ij,kl}=0$ ($U^c_{ij,kl}=0$).

After obtaining the renormalized Green's function $\hat{G}$, we can solve the "Eliashberg" equation,

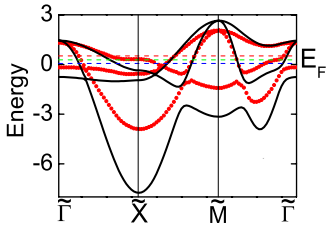

FIG. 2. (Color online) Renormalization of the energy band for $J=0.2U$; the red dotted (black solid) lines are the renormalized (bare) bands. The green, red, and blue dashed lines indicate the Fermi levels for undoping, 10% electron doping, and 20% hole doping, respectively. To show the renormalization more clearly, the energy bands presented here are plotted in the unfolded BZ.

$$\lambda\phi_{mn}(k) = -\frac{T}{N}\sum_{q}\sum_{\alpha\beta}\sum_{\mu\nu} V^{s,t}_{\alpha m,n\beta}(q)G_{\alpha\mu}(k-q)G_{\beta\nu}(q-k)\phi_{\mu\nu}(k-q), \quad (5)$$

where the spin-singlet and spin-triplet pairing interactions $\hat{V}^s$ and $\hat{V}^t$ are given by

$$\hat{V}^s(q) = \frac{3}{2}\hat{U}^s\hat{\chi}^s(q)\hat{U}^s - \frac{1}{2}\hat{U}^c\hat{\chi}^c(q)\hat{U}^c + \frac{1}{2}(\hat{U}^s + \hat{U}^c), \quad (6)$$

$$\hat{V}^t(q) = -\frac{1}{2}\hat{U}^s\hat{\chi}^s(q)\hat{U}^s - \frac{1}{2}\hat{U}^c\hat{\chi}^c(q)\hat{U}^c + \frac{1}{2}(\hat{U}^s + \hat{U}^c). \quad (7)$$

The most favorable SC pairing symmetry corresponds to the eigenvector $\phi_{mn}(k)$ with the largest eigenvalue λ.

The Dyson equation, the self-energy, and the interaction matrix (4) form a closed set of equations and will be solved numerically on 64×64 **k** meshes with 1024 Matsubara frequencies. By symmetry, we set $J'=J$ and use the relation $U=U'+2J$. In the following calculation, the intraorbital Coulomb interaction $U=3.0$ (about 0.3 total bandwidth) is chosen; thus all interaction parameters are given by giving the Hund's coupling J.

III. RESULT AND DISCUSSION

A. Renormalization of band and Fermi surface

We show the renormalized bands for $J=0.2U$ (correspondingly $U'=0.6U$ according to the relation $U=U'+2J$) together with the bare bands in Fig. 2, in which the renormalized bands are calculated from the spectral function $A(\mathbf{k},\omega)=-\frac{1}{\pi}\mathrm{Im}\,G(\mathbf{k},\omega)$ with $G(\mathbf{k},\omega)$ the analytic continuation of the Matsubara Green's function $G(\mathbf{k},i\omega_n)$ by the Padé approximation. The Fermi levels depicted in Fig. 2 are determined by calculating the number of electrons via the renormalized Green's function, and the undoped case is determined from the electron density per site $n=4.0$. It is clearly seen that different bands exhibit different renormalization and the strongest renormalization occurs around the $\tilde{X}$ point. Compared to the bare Fermi level, we find that the renormalized Fermi level is shifted up by $0.3(\approx0.12$ eV) for the undoped case. These features are consistent with the ARPES data.[20,37] We define a total bandwidth renormalization factor as W_B/W_R, where W_B (W_R) denotes the bandwidth of bare (renormalized) band. The renormalization factors for different values of J are shown in Fig. 3(a). It increases from 1.4 to 2.3 when J is increased to be around $0.5U$. In particular, a rapid rise is observed when J is larger than $0.18U$. This shows that the Hund's coupling plays an important role to enhance the renormalization effects.

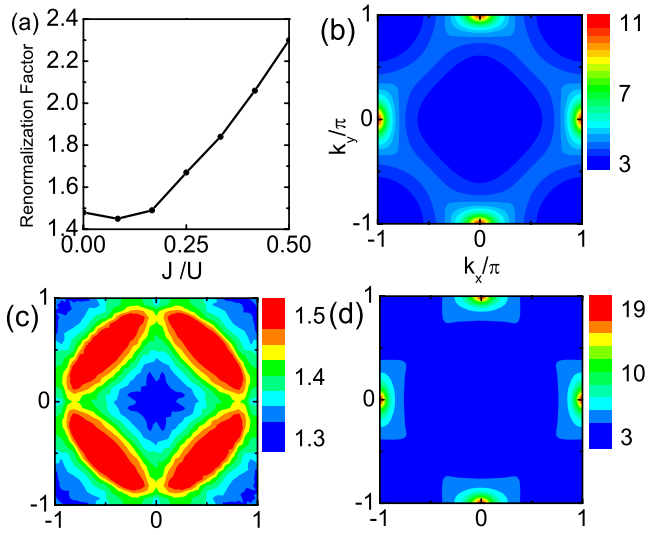

FIG. 3. (Color online) (a) Renormalization factor of total bandwidth for different values of J. (b)–(d) are the spin susceptibilities for $J=0.2U$, $J=0.05U$, and $J=0.3U$, respectively.

For $U>U'$, the spin fluctuation will dominate over the charge fluctuation. In Fig. 3(b),we present the static spin susceptibility $\chi^s(\mathbf{q},\omega=0)=\Sigma_{\mu\nu}\chi^s_{\mu\nu,\mu\nu}(\mathbf{q},\omega=0)$ for $J=0.2U$. It shows four peaks around $(0,\pm\pi)$ and $(\pm\pi,0)$ points, which is in agreement with the neutron-scattering experiments.[6] This arises from the nesting between the hole and the electron pockets connected with the vectors $(0,\pm\pi)$ and $(\pm\pi,0)$, as shown in Fig. 1(b). To show the orbital contribution to the FS, we replot the hole and the electron FS with different colors representing different weights of the three orbitals in Figs. 1(c) and 1(d), respectively. For the nesting part of the FS, it is found that the $d_{yz}+d_{xy}$ orbitals contribute the main weight to the electron pockets and the d_{xz} orbital mainly contributes to the hole pockets. This shows that the spin fluctuation is mainly due to the interorbital particle-hole excitations. As shown in Eq. (3), the Hund's coupling favors the interorbital excitations, so the spin fluctuation around $(0,\pm\pi)$ and $(\pm\pi,0)$ will be enhanced by the increase of J. This is evidenced from the results shown in Figs. 3(c) and 3(d), where the spin susceptibilities for $J=0.05U$ and $J=0.3U$ are presented, respectively. For a small J ($0.05U$), the $(0,\pm\pi)$ spin fluctuation disappears, while for a large J ($J=0.3U$) it is enhanced. Because the band renormalization is increased with the rise of J as discussed above, it suggests that the strong renormalization around the $\tilde{X}$ point mainly comes from the coupling to the spin fluctuation around $(0,\pm\pi)$.

Inspecting the details of the renormalized bands around the $\tilde{X}$ point in Fig. 2, one will find that the energy band near

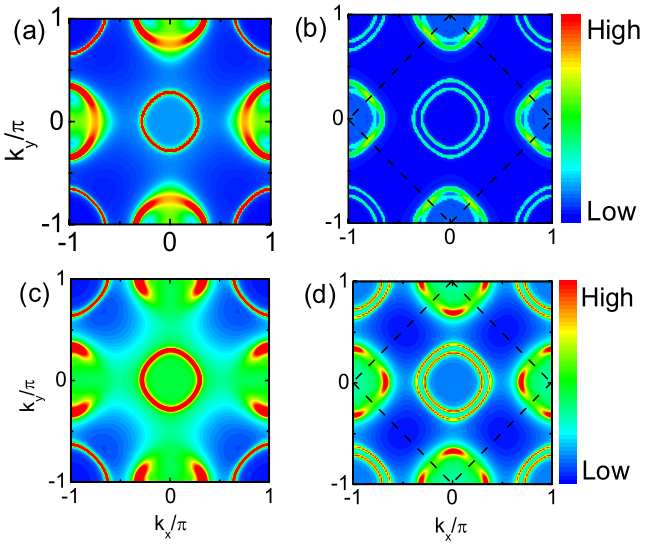

FIG. 4. (Color online) [(a) and (b)] Renormalized FS for 10% electron doping and [(c) and (d)] for 20% hole doping. (a) and (c) are the results shown in the unfolded BZ, while (b) and (d) are the results in the folded BZ.

the Fermi level is renormalized strongly along the $\tilde{\Gamma}$-$\tilde{X}$ direction but less along the $\tilde{X}$-$\tilde{M}$ direction. Another feature is that the band which crosses the Fermi level becomes flat around the $\tilde{X}$ point and the flat portion situates at the bottom of the band along the $\tilde{\Gamma}$-$\tilde{X}$ direction. To identify the FS after renormalization, we calculate the distribution of the spectral weight $A(\mathbf{k},\omega)$ integrated over a narrow energy window $0.02(\approx 8$ meV) around the Fermi level: a method used usually in the ARPES experiments. The results in the unfolded BZ are shown in Fig. 4(a) for 10% electron doping and shown in Fig. 4(c) for 20% hole doping. To compare with experiments, their folded counterparts are shown in Figs. 4(b) and 4(d), respectively. In the undoped case, the Fermi level (the green dashed line) is just slightly below the flatband. Therefore, for the electron-doped case, in which the Fermi level is shifted upward as indicated by the red dashed line for the 10% electron doping, the Fermi level crosses the renormalized bands along both $\tilde{\Gamma}$-$\tilde{X}$ and $\tilde{X}$-$\tilde{M}$ directions. This gives rise to a large complete electron Fermi pocket around the $\tilde{X}$ point as shown in Fig. 4(a) in the unfolded BZ and in Fig. 4(b) in the folded one, which is similar to that predicted by the LDA calculation[23,24,26] and observed in the ARPES experiments.[20,21] However, for the hole-doped case, the Fermi level (the blue dashed line for 20% hole doping) is shifted below the flatband, so that it does not cross the energy band along the $\tilde{\Gamma}$-$\tilde{X}$ direction anymore. Consequently, the complete electron Fermi pocket in the bare case is broken and the spotlike portions are formed around the $\tilde{X}$ point, as clearly shown in Fig. 4(c). After being folded, the electron FS shown in Fig. 4(d) reproduces the experimental results in ARPES measurements.[15,25] We note that due to the band renormalization, the crossing between the two energy bands along the $\tilde{X}$-$\tilde{M}$ directions is shifted up and approaches the Fermi level for 20% hole doping. This crossing gives rise to a large density of states. Therefore it adds an enhancement in the spectral weight around the spotlike portions and makes it easily observed in experiments.

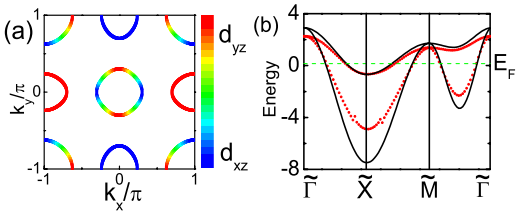

FIG. 5. (Color online) (a) The FS for the two-orbital model and the weight of d_{xz} and d_{yz} orbitals are depicted by different colors. (b) Renormalization of the energy band for the two-orbital model; the red dotted (black solid) lines are the renormalized (bare) bands. The green line indicates the Fermi level for undoping.

The anisotropic band renormalization along $\tilde{\Gamma}$-$\tilde{X}$ and $\tilde{X}$-$\tilde{M}$ directions can be traced to the different orbital weights composing the energy bands along these two directions. Specifically, the energy band near the $\tilde{X}$ point along the $\tilde{X}$-$\tilde{M}$ direction is composed of only the d_{yz} orbital, while that along the $\tilde{\Gamma}$-$\tilde{X}$ direction is a mix of the d_{xy} and d_{yz} orbitals, as shown in Figs. 1(c) and 1(d) in which the different colors represent the weight of the respective orbitals. As noted above, the band renormalization is mainly due to the scattering off the interorbital spin fluctuations composed of the components $\chi_{xz,yz}$, $\chi_{xz,xy}$, and $\chi_{yz,xy}$. We find that the magnitude of the components $\chi_{xz,xy}$ and $\chi_{yz,xy}$ is the same, while it is larger than that of the $\chi_{xz,yz}$. Therefore, the d_{xy} orbital is renormalized most strongly by the spin fluctuation. This suggests that the anisotropic renormalization of the energy band near the $\tilde{X}$ point is orbital dependent.

We note that in the two-orbital model,[30] the energy band near the $\tilde{X}$ point along both directions is composed of one orbital d_{yz}, as shown in Fig. 5(a), so the similar band renormalization is expected. To show this, we have carried out the same calculation for the two-orbital model and the result is presented in Fig. 5(b). Though the strong renormalization still occurs in one of the bands around the $\tilde{X}$ point, no strong anisotropic renormalization between the $\tilde{\Gamma}$-$\tilde{X}$ direction and the $\tilde{X}$-$\tilde{M}$ direction can be seen. Thus, no similar FS reconstruction as observed in the three-orbital model and in experiments[15,25] can be obtained here.

B. Symmetry of superconducting pairing

With the static spin susceptibility, we will further investigate the pairing symmetry mediated by spin fluctuations (Fig. 6). For $J=0.2U$, which is the case with peaks around $(0,\pm\pi)$ and $(\pm\pi,0)$ points in spin fluctuations, we find that the eigenvalue λ has the maximum value in the spin-singlet channel and it is nearly zero in the spin-triplet channel at temperature $T=0.02$. We note that this is not the case considered in Ref. 29, where the spin-triplet state is expected with a larger J (such as $J>U/3$, see also the analysis in Ref. 33). The obtained gap functions of the hole band Δ_{hh} and the electron band Δ_{ee} for 10% electron doping and 20% hole

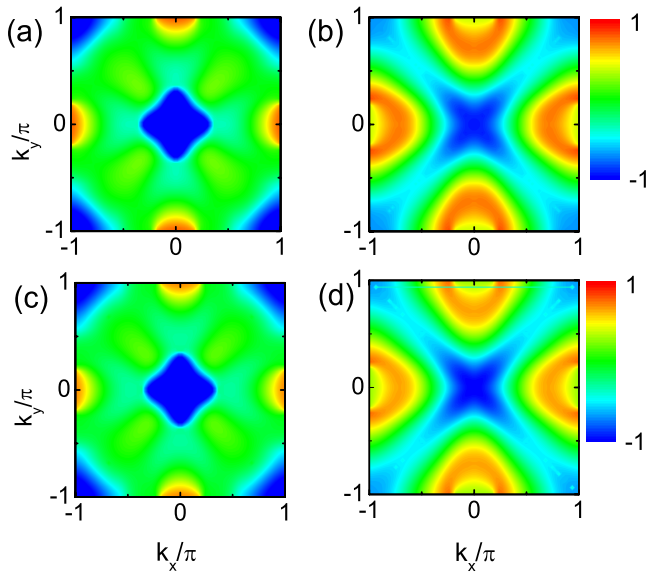

FIG. 6. (Color online) Pairing gap functions in the unfolded BZ for $U=3.0$ with $T=0.02$ for 10% electron doping and 20% hole doping. (a) Δ_{hh} for electron doping. (b) Δ_{ee} for electron doping. (c) Δ_{hh} for hole doping. (d) Δ_{ee} for hole doping.

doping are shown in Figs. 6(a)–6(d). It can be seen that the gap is basically an extended s wave, which is nodeless around all the Fermi pockets and changes sign between the hole pockets and the electron pockets. This result is consistent with the experiment measurements[10–15] and with the calculation based on the two-orbital model.[31] It is noted that the pairing symmetry is similar for both electron-doped and hole-doped systems, although their FS topology is different as discussed above.

Because the spin fluctuation is dominant over the charge fluctuation, the pairing interaction in the spin-singlet channel is positive (repulsive) [see Eq. (6)] and strongest around the wave vectors $\mathbf{Q}$ at which the spin fluctuation has a largest intensity. For a repulsive pairing symmetry, the SC gap will satisfy the condition $\Delta(\mathbf{k})\Delta(\mathbf{k}+\mathbf{Q})<0$ to obtain the largest eigenvalue λ of the "Eliashberg" equation, as can be seen from Eq. (5). For $J>0.1U$, the interband (interorbital) spin fluctuation is dominant and has peaks around $(\pm\pi,0)$ and $(0,\pm\pi)$, which are the nesting wave vectors connecting the hole and the electron Fermi pockets. Thus, the gap will have an opposite sign between these two Fermi pockets. This gives rise to the extended s wave. Because the SC pairing is mediated by the spin fluctuation around $(\pm\pi,0)$ and $(0,\pm\pi)$, which is the same for the three-orbital and the two-orbital models (see Ref. 31), the same pairing symmetry will be obtained based on these two models.

IV. CONCLUSION

In summary, we have investigated the band renormalization, the FS reconstruction, and the symmetry of the superconducting gap in iron-based superconductors using a three-orbital model. A strong anisotropic band renormalization due to the scattering of the interorbital spin fluctuations is found. The band renormalization is shown to be orbital dependent. As a result, the electron Fermi pocket exhibits different topology between electron-doped and hole-doped cases, which provides a natural explanation for the recent ARPES experiments. In addition, we have found that the most favorable superconducting pairing symmetry mediated by the interband (interorbital) spin fluctuations is the extended s wave.

ACKNOWLEDGMENTS

We thank Z. Fang, X. J. Zhou, Q. H. Wang, Z. J. Yao, and H. M. Jiang for many helpful discussions. The work was supported by the NSFC (Grant No. 10525415) and the 973 project (Projects No. 2006CB601002 and No. 2006CB921800).

[1] Y. Kamihara, T. Watanabe, M. Hirano, and H. Hosono, J. Am. Chem. Soc. **130**, 3296 (2008).
[2] X. H. Chen, T. Wu, G. Wu, R. H. Liu, H. Chen, and D. F. Fang, Nature (London) **453**, 761 (2008).
[3] G. F. Chen, Z. Li, D. Wu, G. Li, W. Z. Hu, J. Dong, P. Zheng, J. L. Luo, and N. L. Wang, Phys. Rev. Lett. **100**, 247002 (2008).
[4] C. Wang, L. Li, S. Chi, Z. Zhu, Y. Li Zhi Ren, Y. Wang, X. Lin, Y. Luo, S. Jiang, X. Xu, G. Cao, and Z. Xu, Europhys. Lett. **83**, 67006 (2008).
[5] M. Rotter, M. Tegel, and D. Johrendt, Phys. Rev. Lett. **101**, 107006 (2008).
[6] C. de la Cruz, Q. Huang, J. W. Lynn, J. Li, W. Ratcliff II, J. L. Zarestky, H. A. Mook, G. F. Chen, J. L. Luo, N. L. Wang, and P. Dai, Nature (London) **453**, 899 (2008).
[7] J. Dong, H. J. Zhang, G. Xu, Z. Li, G. Li, W. Z. Hu, D. Wu, G. F. Chen, X. Dai, J. L. Luo, Z. Fang, and N. L. Wang, Europhys. Lett. **83**, 27006 (2008).
[8] Q. Huang, Y. Qiu, Wei Bao, M. A. Green, J. W. Lynn, Y. C. Gasparovic, T. Wu, G. Wu, and X. H. Chen, Phys. Rev. Lett. **101**, 257003 (2008).
[9] M. Rotter, M. Tegel, and D. Johrendt, Phys. Rev. B **78**, 020503(R) (2008).
[10] T. Y. Chen, Z. Tesanovic, R. H. Liu, X. H. Chen, and C. L. Chien, Nature (London) **453**, 1224 (2008).
[11] H. Ding, P. Richard, K. Nakayama, K. Sugawara, T. Arakane, Y. Sekiba, A. Takayama, S. Souma, T. Sato, T. Takahashi, Z. Wang, X. Dai, Z. Fang, G. F. Chen, J. L. Luo, and N. L. Wang, Europhys. Lett. **83**, 47001 (2008).
[12] P. Richard, T. Sato, K. Nakayama, S. Souma, T. Takahashi, Y.-M. Xu, G. F. Chen, J. L. Luo, N. L. Wang, and H. Ding, Phys. Rev. Lett. **102**, 047003 (2009).
[13] L. Malone, J. D. Fletcher, A. Serafin, A. Carrington, N. D. Zhigadlo, Z. Bukowski, S. Katrych, and J. Karpinski, arXiv:0806.3908 (unpublished).
[14] G. Mu, H. Luo, Z. Wang, L. Shan, C. Ren, and H.-H. Wen, arXiv:0808.2941 (unpublished).

[15] L. Zhao, H. Liu, W. Zhang, J. Meng, X. Jia, G. Liu, X. Dong, G. F. Chen, J. L. Luo, N. L. Wang, W. Lu, G. Wang, Y. Zhou, Y. Zhu, X. Wang, Z. Xu, C. Chen, and X. J. Zhou, Chin. Phys. Lett. **25**, 4402 (2008).

[16] K. Matano, Z. A. Ren, X. L. Dong, L. L. Sun, Z. X. Zhao, and G. Q. Zheng, Europhys. Lett. **83**, 57001 (2008).

[17] H.-J. Grafe, D. Paar, G. Lang, N. J. Curro, G. Behr, J. Werner, J. Hamann-Borrero, C. Hess, N. Leps, R. Klingeler, and B. Buchner, Phys. Rev. Lett. **101**, 047003 (2008).

[18] R. T. Gordon, N. Ni, C. Martin, M. A. Tanatar, M. D. Vannette, H. Kim, G. Samolyuk, J. Schmalian, S. Nandi, A. Kreyssig, A. I. Goldman, J. Q. Yan, S. L. Bud'ko, P. C. Canfield, and R. Prozorov, arXiv:0810.2295 (unpublished).

[19] J. D. Fletcher, A. Serafin, L. Malone, J. Analytis, J.-H. Chu, A. S. Erickson, I. R. Fisher, and A. Carrington, arXiv:0812.3858 (unpublished).

[20] D. H. Lu, M. Yi, S.-K. Mo, A. S. Erickson, J. Analytis, J.-H. Chu, D. J. Singh, Z. Hussain, T. H. Geballe, I. R. Fisher, and Z.-X. Shen, Nature (London) **455**, 81 (2008).

[21] C. Liu, T. Kondo, M. E. Tillman, R. Gordon, G. D. Samolyuk, Y. Lee, C. Martin, J. L. McChesney, S. Budko, M. A. Tanatar, E. Rotenberg, P. C. Canfield, R. Prozorov, B. N. Harmon, and A. Kaminski, arXiv:0806.2147 (unpublished).

[22] L. X. Yang, Y. Zhang, H. W. Ou, J. F. Zhao, D. W. Shen, B. Zhou, J. Wei, F. Chen, M. Xu, C. He, Y. Chen, M. Arita, K. Shimada, M. Taniguchi, Z. Y. Lu, T. Xiang, and D. L. Feng, arXiv:0806.2627 (unpublished).

[23] D. J. Singh and M. H. Du, Phys. Rev. Lett. **100**, 237003 (2008).

[24] I. A. Nekrasov, Z. V. Pchelkina, and M. V. Sadovskii, JETP Lett. **88**, 144 (2008).

[25] H. Liu, W. Zhang, L. Zhao, X. Jia, J. Meng, G. Liu, X. Dong, G. F. Chen, J. L. Luo, N. L. Wang, W. Lu, G. Wang, Y. Zhou, Y. Zhu, X. Wang, Z. Xu, C. Chen, and X. J. Zhou, Phys. Rev. B **78**, 184514 (2008).

[26] L. Boeri, O. V. Dolgov, and A. A. Golubov, Phys. Rev. Lett. **101**, 026403 (2008).

[27] I. I. Mazin, D. J. Singh, M. D. Johannes, and M. H. Du, Phys. Rev. Lett. **101**, 057003 (2008).

[28] F. J. Ma and Z.-Y. Lu, Phys. Rev. B **78**, 033111 (2008).

[29] P. A. Lee and X.-G. Wen, Phys. Rev. B **78**, 144517 (2008).

[30] S. Raghu, X.-L. Qi, C.-X. Liu, D. J. Scalapino, and S.-C. Zhang, Phys. Rev. B **77**, 220503(R) (2008).

[31] Z.-J. Yao, J.-X. Li, and Z. D. Wang, arXiv:0804.4166, New J. Phys. (to be published).

[32] Y. Ran, F. Wang, H. Zhai, A. Vishwanath, and D.-H. Lee, Phys. Rev. B **79**, 014505 (2009).

[33] W. Chen, K.-Y. Yang, Y. Zhou, and F.-C. Zhang, Phys. Rev. Lett. **102**, 047006 (2009).

[34] K. Seo, B. A. Bernevig, and J. P. Hu, Phys. Rev. Lett. **101**, 206404 (2008).

[35] M. Daghofer, A. Moreo, J. A. Riera, E. Arrigoni, D. J. Scalapino, and E. Dagotto, Phys. Rev. Lett. **101**, 237004 (2008).

[36] N. E. Bickers, D. J. Scalapino, and S. R. White, Phys. Rev. Lett. **62**, 961 (1989); N. E. Bickers and D. J. Scalapino, Ann. Phys. (N.Y.) **193**, 206 (1989); T. Takimoto, T. Hotta, and K. Ueda, Phys. Rev. B **69**, 104504 (2004).

[37] H. Ding, K. Nakayama, P. Richard, S. Souma, T. Sato, T. Takahashi, M. Neupane, Y.-M. Xu, Z.-H. Pan, A. V. Federov, Z. Wang, X. Dai, Z. Fang, G. F. Chen, J. L. Luo, and N. L. Wang, arXiv:0812.0534 (unpublished).